# Angular and temperature dependence of the magnetic circular dichroism in 4*d* core-level photoemission from Gd(0001)

R. Denecke,*,† J. Morais,*,‡ and R. X. Ynzunza*,§
*Materials Sciences Division, Lawrence Berkeley National Laboratory, Berkeley, California 94720*

G. H. Fecher
*Johannes Gutenberg Universität, Institut für Physik, D-55099 Mainz, Germany*

J. G. Menchero,‖,¶ J. Liesegang,** and J. Kortright
*Materials Sciences Division, Lawrence Berkeley National Laboratory, Berkeley, California 94720*

Z. Hussain
*Advanced Light Source, Lawrence Berkeley National Laboratory, Berkeley, California 94720*

C. S. Fadley*
*Materials Sciences Division, Lawrence Berkeley National Laboratory, Berkeley, California 94720*
(Received 20 July 2001; revised manuscript received 21 February 2002; published 21 June 2002)

We present experimental and theoretical results for the angular and temperature dependence of magnetic circular dichroism in Gd 4*d* core-level photoelectron emission from a Gd(0001) surface in both normal and off-normal directions and with azimuthal variation. Two theoretical approaches are used to model this data: a single electron theory with full multiple scattering of the outgoing photoelectron and a full-relativistic many-electron theory with single scattering only. Thermal effects due to atomic vibrations and the excitation of initial-state multiplets are also included. For normal emission, we find smooth free-atom-like angular variations in emission intensity, while for off-normal emission, deviations from a purely atomic model due to photoelectron diffraction effects are seen that are well predicted by photoelectron diffraction theory. We also compare dichroism measurements using two different approaches (fixed magnetization with variable light helicity and fixed light helicity with rotated sample magnetization) and find significant differences between them that are also well predicted by theory. The angular dependence of magnetic circular dichroism for a specific set of Gd 4*d* multiplet states has also been measured with high electron energy resolution ($\leqslant$100 meV), permitting a state-specific decomposition of the dichroism. Such state-resolved dichroism is found to be very well described by our many-electron approach. Finally, we present temperature-dependent magnetic circular dichroism (MCD) data for 4*d* emission that should permit the study of near-surface magnetic phase transitions, and discuss the relationship of such MCD measurements to magnetization. Some future prospects and applications of such core-photoemission dichroism measurements are discussed.

DOI: 10.1103/PhysRevB.65.245421 PACS number(s): 61.14.Qp, 75.50.Cc, 78.20.Ls, 79.60.Dp

## I. INTRODUCTION

Magnetic dichroism in core-level photoelectron emission from solids represents an element-specific probe of surface and interface atomic structure and magnetic order that is now finding wider use.[1–3] It is especially attractive because it does not involve time-consuming spin-polarization analysis, as compared to some other photoemission techniques used to study magnetism.[4] This feature is shared with x-ray magnetic circular dichroism (XMCD) in absorption spectroscopy, a somewhat more bulk sensitive technique which is used to determine magnetic moments by employing various sum rules.[5,6] In its most precise form, magnetic circular dichroism in angular distributions (MCDAD) measures such effects by using photoelectrons excited with circularly polarized radiation, and noting that photoemission intensity with right-circularly polarized (RCP) light is different from that with left-circularly polarized (LCP) light.[1]

The earliest experiments in magnetic circular dichroism (MCD) using photoemission were conducted by Lubell and Raith[7] on oriented Cs atoms; these provided experimental verification of Fano's proposal of induced spin polarization if circularly polarized light is used for excitation.[8] From the atomic point of view, any atom with an unfilled shell, in particular with unpaired electrons, is magnetic. If Cs atoms are state selected (e.g., $^2S_{1/2}$, $M_J=-\frac{1}{2}$) by a Stern-Gerlach field and the orientation is preserved in a homogeneous magnetic field, one will measure a difference in the emitted intensity if switching either the direction of the magnetic field or the helicity of the photons, even if the spin of the electrons is not measured. We review this classic result to point out that magnetic dichroism in photoemission is at first sight an atomic phenomenon and note that atomic theoretical models have been used successfully to explain many aspects of MCD data.[9–13] Such models will not, however, predict the correct intensities or the resulting dichroism or temperature dependence of measurements taken from ferromagnetic solid samples unless the basic elements of the solid state are included. This includes, for example, the scattering of the photoelectron in leaving the sample, resulting in photoelec-

 

tron diffraction (PD), an effect that we explicitly consider in the present study.

It should also be mentioned that there exists a circular dichroism in the angular distribution of photoelectrons (CDAD), even for nonmagnetic or nonmagnetized samples.[14–19] These effects are always linked to photoelectron diffraction, they prevail in the data presented here, and they should be taken into account for a fully quantitative analysis.[15,16] It was recently shown[31] that the nonmagnetic part of CDAD influences both the magnetic dichroism and the spin polarization of photoelectrons. In particular it was shown that CDAD is a more general phenomenon being independent of the electron spin or the sample magnetization. The calculations reported in the present work will include such effects. It should be noted that magnetic dichroism may also be measured in photoemission using linearly polarized radiation (MLDAD),[20] as well as unpolarized radiation from laboratory sources (UMDAD, also referred to as MUDAD in some papers).[21–23]

The spin-integrated photoelectron intensity in a certain emission direction also in general depends on the direction of the magnetization in a magnetic material. In fact, if the magnetization lies in a mirror plane perpendicular to the surface, then inverting its direction can provide a second way of measuring MCD. This difference may be indicated by calling this type of experiment circular magnetic dichroism in angular distribution (CMDAD), following suggestions by Venus[24] and Fecher *et al.*[25] As has been shown in previous publications,[26] there are certain angular dependencies associated with MCD in photoemission which come from the interplay of the different vectors involved (namely the magnetization direction, the polarization of the incoming light, and the electron wave vector) and from interference effects between different photoemission channels allowed by dipole selection rules. Such angular-dependent effects have, for example, been measured in magnetic circular or linear dichroism in angular distribution (MCDAD or MLDAD).[27,28] Photoemission electron microscopy (PEEM) techniques have also used this angular variation as a contrast mechanism.[29] Beyond this, it is well known that by varying the emission direction of the photoelectrons one may also probe the geometric structure of the sample. Consequently, dichroism data have to be interpreted also in terms of photoelectron diffraction,[30] so as to allow for final-state scattering of the photoelectrons in leaving the sample surface. Such diffraction effects have been shown to be important in understanding CDAD,[16–18,31] MLDAD,[28] MCDAD,[32] or UMDAD (Refs. 23 and 33) measurements.

In this work, we present experimental data and theoretical calculations for magnetic and circular dichroism in $4d$ core-level photoemission from Gd(0001). Although very strong dichroism in both $4d$ and $4f$ core-level spectra has been observed before for this system,[2] leading to considerable interest in it for magnetic studies,[34,35] its angular dependence has not been studied in detail previously, particularly in comparison to different levels of theoretical description. Furthermore, we have been able to resolve the dichroism according to the individual $4d$-hole atomiclike multiplets involved, and also to study the temperature dependence of such MCDAD, with the latter providing a useful tool for studying magnetic transition temperatures in the future. Such temperature-dependent measurements are especially interesting for Gd, since there are several reports of an enhanced transition temperature for the surface,[36–41] and a recent theoretical discussion of its possible origin in interlayer relaxation,[42] but still some controversy over its cause. Since photoelectron spectroscopy can be tuned to be more or less surface sensitive by choosing the correct energy, core-level MCDAD thus offers a powerful way to study such effects. One should, however, also keep in mind that the dichroism itself may strongly depend on the photoelectron energy, as has been shown (e.g., for MLDAD) for thin Gd layers on Fe.[43] These results should thus provide a firmer foundation for the analysis and use of such dichroism in photoemission for the study of magnetic systems.

## II. EXPERIMENT

The experiments have been performed on bend-magnet beamline 9.3.2 at the Advanced Light Source (ALS) in Berkeley, CA,[44] using the advanced photoelectron spectrometer/diffractometer (APSD) end station.[45] Photoelectron spectra were measured with a Scienta SES-200 electron analyzer, with an overall photon-plus-analyzer energy resolution of about 0.1 eV and angular resolution of about $\pm 5°$. A special feature of this end station is the ability to rotate the analyzer relative to the incoming photon beam and independently of the sample. This enabled a change of the electron emission angle without changing the light incidence angle on the sample. All spectra shown have been taken at a photon energy of about 440 eV, yielding Gd $4d$ photoelectron energies of 298 eV for the dominating $^9D_6$ line of the multiplet, similar to previous measurements.[12] This energy is sufficiently high to assure that the photoemission process is taking place in the sudden limit, as assumed in our subsequent many-electron theoretical treatment. The helicity of the photons may be chosen at this beamline by moving an aperture above or below the plane of the storage ring, with the degree of circular polarization being about 80–85%.[44] In the experiments presented here, we have largely used RCP light and have obtained the CMDAD signal by inverting the magnetization direction; however, in some measurements we also used a fixed magnetization direction and measured the MCDAD by switching the light helicity. For certain geometries, both experiment and theory show significant differences between these two procedures, as discussed further below.

The samples used were thin films of Gd evaporated at room temperature onto a clean W (110) substrate, with the pressure being about $3\times10^{-10}$ mbar during evaporation. The thickness of the Gd films in monolayers (ML's) was chosen to be 100 ML's (287Å) in order to ensure in-plane magnetization,[46–49] and final annealing at 700 K to ensure monatomically flat surfaces.[41,50] The cleanliness and crystalline order of the substrate and the final films were checked before and after MCD measurements by x-ray photoelectron spectroscopy (XPS) and low-energy electron diffraction (LEED). The Gd films have been studied with remanent in-

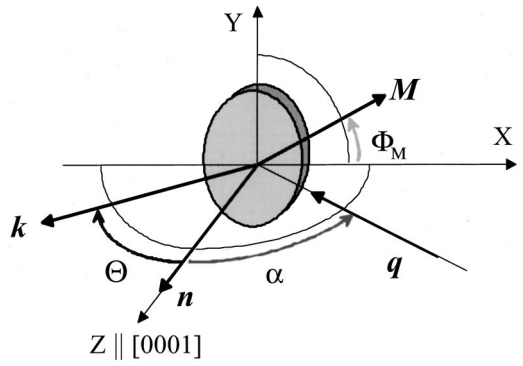


FIG. 1. The general experimental geometry as described in the text.

plane magnetization, as induced by an *in situ* magnetic field of about 200 G applied along a high-symmetry direction of the $[10\bar{1}0]$ type containing a mirror plane of the crystal. Unless temperature was specifically a variable, the samples were kept at about 250 K throughout the measurements, well below the transition temperature for films with this thickness ($T_c = 292$ K).[51]

During photoemission measurements, the light impinged on the sample with an angle of incidence of $\alpha = 70°$, that is 20° relative to the surface plane. The experimental geometry is shown in Fig. 1; the photon incidence direction **q**, the surface normal **n**, and the photoelectron wave vector **k** all lie in a plane. The photoelectrons were collected either in normal emission or off-normal emission at a polar angle of $\Theta = 20°$ with respect to the surface normal, simply by moving the electron analyzer. The sample was rotated stepwise about its surface normal so as to vary the azimuthal emission angle with respect to the crystal. Dichroism measurements via inversion of the magnetization were done simply by rotating the sample by 180° around the surface normal. The azimuthal angle varied in the angle-dependent spectra shown below ($\Phi_M$) is thus also the angle between the magnetization directions and the plane of incidence containing **q**, **n**, and **k**. Typical measured spectra and the CMDAD result derived from them, are shown in Figs. 2(a) and (b), with more detailed discussion below. Further experimental details can be found elsewhere.[52]

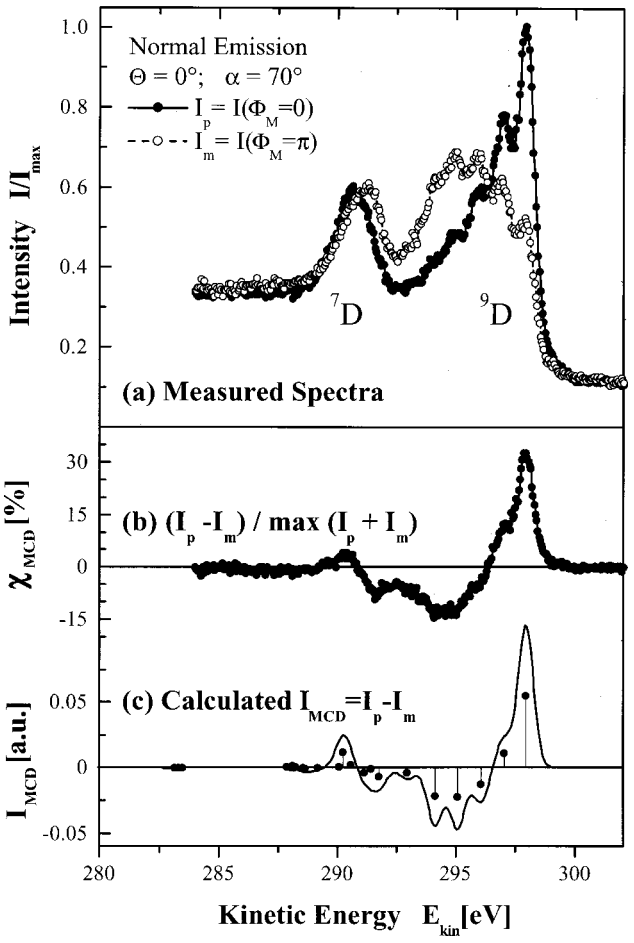


FIG. 2. Magnetic dichroism in Gd 4*d* emission. (a) Gd 4*d* core-level photoemission spectra taken at a photon energy of about 440 eV with normal emission and using right circular polarized light. The solid-line spectrum (filled circles) was taken with the sample magnetization maximally parallel to the azimuth of the light incidence direction ($\Phi_M = 0$), and the dotted-line spectrum (open circles) with a maximally antiparallel arrangement ($\Phi_M = 180°$). (b) The curve plus data points represent the normalized difference or CMDAD asymmetry of the data in (a) (for details see text). (c) Result of a theoretical atomic calculation including multiplet splitting, according to the theory described in Sec. III B, which shows excellent detailed agreement with the curve in (b).

## III. CALCULATIONAL DETAILS

We have here used two different theoretical approaches to simulate the magnetic dichroism associated with Gd 4*d* emission: a nonrelativistic single electron model and a full-relativistic many-electron model. As an initial comment on the difference between these two approaches, it may be noted that the number of input parameters increases tremendously in the full-relativistic calculations. In the nonrelativistic case, we need for the 4*d* emission only two complex matrix elements for final *p* and *f* channels and $l_{max}+1=7$ scattering phases if we allow, for example, $l_{max}=6$ as a maximum of the orbital momentum of the partial waves for the scattering. At the same time we need in the relativistic full potential case up to 30 complex single-particle matrix elements and $2(l_{max}+1)^2=98$ scattering phases to account for the total angular momentum *j* and the lifting of the $m_j$ degeneracy. This results under the same conditions in about 16 times more parameters that have to be calculated self-consistently. In addition, this estimation does not include the different kinetic energies of the particular lines of the multiplet.

Both types of calculations use a three-step scheme, which has already been used to describe core-level photoemission very well. The first model, which has briefly been discussed before,[52] treats spin-orbit splitting and exchange splitting in the initial state as perturbation and uses multiple-scattering cluster diffraction calculations to describe the final-state outgoing electron; however, since it is a single electron theory, a distinct multiplet description is not used. By contrast, calculations are also presented treating the multiplet nature in a

relativistic many-electron way, and, moreover, dealing with full potential relativistic scattering, but in a simpler single-scattering picture of the outgoing electron. The two approaches discussed here thus complement the recent work on MCD in $3p$ photoemission from Fe and Ni by Henk *et al.*,[53] which uses a single electron approach but with full-relativistic multiple scattering. We will next introduce both calculation schemes and compare their results and complementary conclusions.

### A. Single electron, multiple-scattering cluster calculations

In this section we will discuss multiple-scattering cluster calculations including spin-orbit and exchange splitting in the initial state.[54–56] The diffraction effects were calculated using the Rehr-Albers separable representation of the scattering matrix.[57] The MCD was calculated using the single electron approach discussed by Menchero for an $l=1$ core level,[13] but generalized here to include emission from an $l=2$ core level. We have not in this approach considered the detailed multiplet splitting, spin and orbital angular momentum couplings, and configuration interaction effects that have, for example, been included in previous modeling of Gd $4d$ MCDAD data at a fixed emission direction,[12] which we will term purely atomic. Rather, we have approximated in a first step all of these effects through a simple spin-orbit splitting of the $4d_{3/2}$ and $4d_{5/2}$ levels and an effective exchange field splitting of the four $m_j$ sublevels in $\frac{3}{2}$ and the six sublevels in $\frac{5}{2}$, as obtained previously from similar analyses of $2p$ spectra of $3d$ metals.[1,13,58] Therefore, although the single electron approach considered here is not intended to reproduce the complicated multiplet structure of the individual photoelectron energy distribution curves contributing to MCDAD, we do expect that it should provide a simple description of the overall ensemble of states and the angular variation of its intensity and dichroism, explaining most features induced by photoelectron scattering. By thus treating the core level as having two spin-orbit split parts, each of which is split by the exchange interaction into $(2j+1)$ states, the intensity for any of the resulting ten $jm_j$ states and for any photon polarization may thus be determined. Note that since we do not intend to actually predict spectral intensities as a function of energy, we do not in fact have to specify the spin orbit or exchange splitting quantitatively. It should be emphasized, however, that we have in this approach included both the $p$ and $f$ final-states channels allowed in $d$ emission and that we have explicitly included the interference between these channels. In fact, it is found that this so-called cross-channel interference accounts for most of the angular variations seen in the atomic theoretical models of all types of magnetic dichroism.[10,13,23,58,59]

Following the scheme as used by Menchero,[13] we finally obtain the overall CMDAD magnitude from

$$\chi^{*}_{\mathrm{CMDAD}} = 100 \cdot \frac{\Sigma_{(j,m_j)}[I(j,m_j) - I(j,-m_j)]}{\Sigma_{(j,m_j)} I(j,m_j)}, \qquad (1)$$

with the sum in the numerator being only over $jm_j$ states with $m_j > 0$. This procedure is therefore very similar to the analysis of the experimental data.

To simulate the Gd(0001) surface, we used a cluster with four layers of atoms, and an emitter placed in each of the layers. Each cluster consists of 182 atoms and has threefold rotational symmetry about the surface normal; however, to account for the steps that are present in any macroscopic sample and the two domain types thus resulting, we have used two cluster types, with *ABAB* and *BABA* stacking. When intensities are averaged over both cluster types, the system acquires the sixfold rotational symmetry that is observed experimentally. Multiple scattering was allowed up to seventh order.

The kinetic energy of the photoelectrons in the crystal was taken to be 295 eV; i.e., close to the average measured kinetic energy for the Gd $^{7,9}D$ multiplet. An inner potential of 10 eV was used, so that the electron kinetic energy inside the surface was increased by this amount in the calculations, and refraction effects at the surface were included. The photoelectron inelastic scattering was included via an attenuation length of 8 Å as determined from the so-called universal curve for elements due to Seah and Dench,[60,61] and checked against the value calculated from the ''TPP-2M'' formula of Tanuma, Powell, and Penn.[62] The light was right-elliptically polarized ($p$ like) with Stoke's parameters $s_1 = 0.45$, $s_2 = 0.0$, and $s_3 = 0.89$. The angular broadening was chosen to be $\pm 5°$ to simulate the resolution of the electron analyzer.

The scattering phase shifts were determined using muffin-tin potentials.[41] In our calculations we used the paramagnetic, nonrelativistic phase shifts; i.e., we have neither allowed for exchange nor for spin-dependent scattering. When test cases were run with pseudoferromagnetic phase shifts using different scattering potentials for spin-up and spin-down electrons but neglecting spin-orbit interaction, the intensities, and asymmetries changed by only in the order of about 1%. Such differences may be safely neglected when compared to the calculated asymmetries, which are of the order of 50%. The individual channel matrix elements ($R_f$) and phase shifts ($\delta_f$) for the two final-state channels were determined using the Manson program as described by Goldberg, Fadley, and Kono,[63] with the result: $R_{d,p} = 0.0270$, $R_{d,f} = 0.0664$, $\delta_{d,p} = 2.576$, and $\delta_{d,f} = 4.201$. It should be noted that the relative energy spread of the $^9D$ part of the multiplet is less than 1.5% in the measurements. We checked by calculations using a ''wrong'' kinetic energy (reversed level ordering) that a maximum difference in the asymmetries of about 2% may occur at a 60% level (depending on the type of dichroism, angles, etc.), which is less than the estimated experimental error. The explanation is that none of the radial integrals or phases changes more than 1% within the energy range of the $^9D$ part of the multiplet.

### B. Many-electron, full-relativistic single scattering cluster calculation

As a starting point for the second set of calculations we use the multiplet theory of Cowan.[64] That is, we calculated the energy spectra using intermediate coupling (**LSJ** or $\mathfrak{J}$**J**) by treating both spin-orbit and exchange splitting as perturbations. We use in the following always the easier to handle and more common Russel-Saunders notation $^{2S+1}L_J$ even if

starting from **jj** and not from **LS** coupling. For the purpose of the first step of the calculations, Cowan's program[65] was modified to account only for such intermediate states during the coupling of the electrons that give $^8S_{7/2}$ for the state of the first parity (as defined by Cowan in Ref. 64) and $^{7,9}D_J$ (or their $\mathfrak{J}\mathbf{J}$ coupled pendants) for the core hole before coupling the free electron to the created ion. The latter coupling results in the overall state of second parity. The restrictions to the $^8S$ ground state are also chosen to ensure that the restrictions of the sudden approximation are justified. Because we would like to perform relativistic calculations for the angular distributions, we did not fit the spin-orbit or atomic exchange parameters to the experiment but used instead the calculated values as given in Ref. 64. These values are found to lead to a good agreement between the measured and calculated spectra with respect to the splitting of the states and their intensity [see Fig. 2(c) and later discussion of it]; and it should be noted that by starting with the Dirac equation there is no possibility to parametrize the spin-orbit interaction, because it is an intrinsic property.

As reported previously,[25] the use of nonrelativistic $|l,s\rangle$ wave functions leads to unsatisfactory results in explaining the angular dependency of the CDAD or MCDAD in emission from rare-earth metals. In particular such wave functions even fail to explain the Fano effect.[7] Therefore we chose a relativistic $|j,m_j\rangle$ basis set for the calculation.

The dipole matrix element for excitation of atoms with coupled electrons in the sudden approximation is[9,64]

$$D_{if}=\sum_{M_J,m_j}\langle\Phi_f|\underline{l}^\dagger|\Phi_i\rangle\cdot\langle\phi_f|\boldsymbol{\varepsilon}\bullet\mathbf{r}|\phi_i\rangle. \tag{2}$$

Here $\Phi_i$ and $\Phi_f$ are the states describing the coupled initial state and the coupled final state after creation of a core hole in the shell with angular momentum $l$, and $\underline{l}^\dagger$ is the associated hole creation operator. The remaining part is the usual length form of the dipole matrix element in a single-particle description $M_{if}=\boldsymbol{\varepsilon}\cdot\langle\phi_f|\mathbf{r}|\phi_i\rangle$, where the photon polarization is separated out because it does not depend on the radial integration. The overlap integral $\langle\Phi_f|\underline{l}^\dagger|\Phi_i\rangle$ is related to the spectral function in the many-body treatment of photoemission.

We use an $RE^{3+}$ rare-earth ion as starting point, that is all couplings to the electrons going to bands ($6s^2$ and $5d^1$) are neglected. Therefore the following states for the coupled initial and excited states of the ion are used (see also Refs. 9 and 64):

$$\Phi_i=|\mathrm{RE}^{3+}4f^y nl^x LSJ\ \ M_J\rangle;$$

$$\Phi_f=|\mathrm{RE}^{4+}4f^y nl^{x-1}\underline{LSJ}\ \ \underline{M}_J\rangle, \tag{3}$$

where $x$ is the initial occupation of the $nl$ subshell being ionized and $y$ is the occupation of the open $4f$ shell. Here we have in particular $x=10$ for creation of a core hole in the filled $4d$ subshell and $y=7$ in the case of Gd. The states may be recoupled as described in Ref. 64, if necessary. In $\mathfrak{J}\mathbf{J}$ coupling we remove the electron from a shell with total angular momentum $j=l\pm s$ rather than $l$. Inserting these states into $D_{if}$ we find that the overlap portion of the matrix element for transitions from the initial to the final state is given by

$$\langle\Phi_f|\underline{j}^\dagger_{m_j}|\Phi_i\rangle=\langle\underline{\gamma}\underline{J}\underline{M}_J|\underline{j}^\dagger_{m_j}|\gamma JM_J\rangle$$

$$=\frac{-1^{j+m}}{\sqrt{2J+1}}C^{\underline{J}\underline{M}_J}_{JM_J,jm_j}\langle J\|j^\dagger\|\underline{J}\rangle \tag{4}$$

with $C^{\underline{J}\underline{M}_J}_{JM_J,jm_j}$ being a Clebsch-Gordan coefficient and $\langle J\|j^\dagger\|\underline{J}\rangle$ being the reduced matrix element of the electron creation operator. Here the hole creation operator $\underline{j}^\dagger_{m_j}$ becomes replaced by the fermion creation operator $j^\dagger$, and $\gamma$ and $\underline{\gamma}$ are used as substitutes for all quantum numbers being omitted for convenience. The reduced matrix element of the electron creation operator is simply $\langle J\|j^\ddagger\|\underline{J}\rangle=\sqrt{x(2J+1)}$. $x=2j+1$ is the initial occupation of the ionized shell with total angular momentum $j$, here we have in particular $x=6$ for $d_{5/2}$ and $x=4$ for $d_{3/2}$.

The square of the Clebsch-Gordan-coefficients in Eq. (4),

$$n(j,m_j)=[C^{\underline{J}\underline{M}_J}_{JM_J,jm_j}]^2, \tag{5}$$

may be interpreted as an effective partition number, giving the probability that a single-particle initial state $|j,m_j\rangle$ takes part in the transition from the ground state $\Phi_i$ into the final core-hole state $\Phi_f$. This partition number determines also the possible free-electron states $\phi_f$ of Eq. (2) via the dipole selection rules.

For clarity here, we note that the terms initial and final state have slightly different meanings in the single-particle and many-particle theory. Here, we use the term ''initial'' for a unique many-particle electronic state of the atom or ion before photoexcitation (usually the ground state with the bound electron) and the term ''final'' for all states after the photoexcitation (the excited state of the ionized atom with the final free electron). Looking ahead, however, we note that the different magnetic sublevels of the initial state may in fact be populated if the temperature is high enough.

In order to calculate the angular resolved intensities and the MCDAD, and in particular to include photoelectron diffraction, we need the angular dependent amplitudes rather than the intensities and energies as calculated by Cowan's program. The photon-polarization resolved single-particle matrix elements $\langle\phi_f|\mathbf{r}|\phi_i\rangle$ are defined by the radial integrals $R_{i,f}=\langle\phi_f|r|\phi_i\rangle$ and final state phases $\delta_{i,f}$. Both were calculated in the averaged configuration approximation using a relativistic self-consistent field program accounting for the single electron transitions $4d_{3/2}\rightarrow\varepsilon(p_{1/2},p_{3/2},f_{5/2})$ and $4d_{5/2}\rightarrow\varepsilon(p_{3/2},f_{5/2},f_{7/2})$. We find approximately (all calculations are using the kinetic energies as observed in the experiment for each individual line) for the $^7D$ part of the multiplet the radial integrals $R^{3/2,1/2}_{d,p}=0.0723$, $R^{3/2,3/2}_{d,p}=0.0667$, $R^{3/2,5/2}_{d,f}=0.129$, and the final-state phases $\delta^{3/2,1/2}_{d,p}=2.82$, $\delta^{3/2,3/2}_{d,p}=2.64$, $\delta^{3/2,5/2}_{d,f}=3.91$, that are slightly different from those of the $^9D$ part: $R^{5/2,3/2}_{d,p}=0.0678$, $R^{5/2,5/2}_{d,f}=0.138$, $R^{5/2,7/2}_{d,f}=0.135$, and $\delta^{5/2,3/2}_{d,p}=2.62$, $\delta^{5/2,5/2}_{d,f}=3.91$, $\delta^{5/2,7/2}_{d,f}=3.89$ (the lower indices $l_1$, $l_2$ assign the orbital and the upper indices

$j_1$, $j_2$ the total angular momenta of the initial- and final-state quantum numbers). It should be noted that the parameters depend not only on the kinetic energy for a particular transition but also on $m_j$ (and not only on $l$ and $j$) due to the crystalline symmetry and the magnetization. The relative phases are close to the values derived in the nonrelativistic approximation (see above). Larger differences in the absolute values of the radial integrals are due to a different definition of constants entering the matrix element and the total cross section. The angular dependent photoelectron amplitudes derived by means of those final states are used as a starting point for the spin-dependent single scattering cluster calculations as described in Refs. 19, 31, and 66.

The amplitudes of the outgoing photoelectrons are described in the single-scattering cluster approximation by a coherent superposition of the direct wave with all waves scattered singly by the atoms of a given cluster. In contrast to previous approaches, the amplitudes $\Psi_0$ of the direct and $\Psi_i$ of the scattered waves here are spinors:

$$\Psi = \Psi_0(\hat{k}) + \sum S_i(\vartheta_i, \varphi_i)\Psi_i(\hat{k}, \hat{r}_i)$$

$$= \begin{pmatrix} \alpha_0 \\ \beta_0 \end{pmatrix} + \sum \begin{pmatrix} S_i^{11} & S_i^{12} \\ S_i^{21} & S_i^{22} \end{pmatrix} \begin{pmatrix} \alpha_i \\ \beta_i \end{pmatrix} \cdot \Gamma_i, \qquad (6)$$

where we have accounted for the *large* component of the relativistic wave functions only. The amplitudes depend on the direction of emission $\hat{\mathbf{k}}$ and the position of the atoms $\hat{\mathbf{r}}_i$ for the direct and the scattered waves, respectively. The usual scattering amplitude is replaced by a $2\times2$ matrix which depends on the polar and azimuthal scattering angles. Due to the magnetization of the sample, the scattering amplitude need no longer to be of cylindrical symmetry with respect to the direction of the incoming electrons. $\Gamma_i$ accounts for inelastic processes and differences in the path between the emitting and scattering atoms. The intensity is finally given by the absolute square of the amplitudes averaged over both spin directions, since the spin is not resolved in the present measurements. The scattering phases used for the photoelectron diffraction step are calculated by a relativistic full potential method including exchange, as is well known from single-step photoemission calculations.[67,68] The potential used to determine the relativistic scattering phases is self-consistently derived. Our algorithm allows inclusion of the full solid-state symmetry and no assumption of spherical symmetry as in muffin-tin methods needs to be made. The combination of crystal field and exchange interaction (due to the magnetization of the sample) results in scattering phases that depend on the total angular momentum $j$ and its projection $m_j$ and not only on the orbital angular momentum $l$. As a result, all four components of the scattering matrix are different.

The amplitudes $\Psi_0$ and $\Psi_i$ of the emitted electrons are calculated from full-relativistic single-particle matrix elements [similar to the second part of Eq. (2)] using the phases and radial integrals as given above. The final amplitudes and intensities so derived are mixed according to the multiplet description as given above in order to find the final results for the intensity and the magnetic dichroism of the lines of the multiplet. In principle this mixing may be performed on the single electron states from the above-mentioned calculation as well so as to yield multiple-scattering effects.

Multiple scattering is omitted here on the one hand because of the tremendous number of scattering phases needed and on the other hand because it influences the dichroism much less than the intensity itself, which may more easily be found from symmetry considerations as shown in Ref. 31. Overall, the results given below show that a three-step model with single scattering is sufficient to explain the present data. The calculations to be compared later with the experimental results were performed in the geometry as described in Sec. II. In particular, a cluster of 50 atoms was used, allowing emission from the four topmost layers. As in the spin-independent multiple-scattering calculations, both possible stacking orders *ABAB* and *BABA* of the hcp crystals are accounted for, resulting in eight different geometrical configurations overall. The topmost layer was assumed to couple ferromagnetically to the bulk.

One also has to include temperature variation if comparing the results of calculations with measurements. The temperature influences the intensities as well as the dichroism mainly for two reasons. First, the lattice vibrations will smear out the scattering induced features in the intensity. Second, the orientation of the atoms is lowered by thermal motion of the atomic magnetic moments. If the latter effects are not accounted for, the calculations correspond to measurements at $T=0$ K.

The temperature effect on the scattering caused by thermal fluctuations may easily be allowed for by introducing a Debye-Waller factor $W_i$ in the scattering matrix:[69,70]

$$S_i(T) = S_i \cdot W_i(T), \qquad (7)$$

where

$$W_i = \exp\{-w_a[1-\cos(\Theta_i)]\}$$

and $\Theta_i$ is the scattering angle at the $i$th atom. In addition to the temperature, the Debye-Waller factor includes the mean momentum transfer and displacement associated with the kinetic energy of the electrons and the mass $m_a$ of the atom. The exponential factor for the correction is given by

$$w_a = \frac{3E_{\mathrm{kin}}T}{m_a k_B \theta_D^2} = 1.78\times10^{-3}\cdot T[\mathrm{K}], \qquad (8)$$

assuming a kinetic energy of about $E_{\mathrm{kin}}=295$ eV as in the experiments, and a Debye temperature for Gd of $\theta_D = 200$ K as found in the literature.[71] Extensions of the model to include lattice vibrations may be found in Ref. 72.

Calculating the second effect of temperature on the orientation of the atoms in the initial state is a little more complicated. It is assumed that we are in the thin-film limit, so that only one single magnetic domain exists. Without external field and below the Curie temperature $T_C$, the magnetization is given by the saturation magnetization $M_{\mathrm{sat}}(T)$ depending on the temperature. In the molecular field approximation, this magnetization is connected to an internal magnetic field $B(T)$ acting on each atom of the domain. If $\lambda$ is the molecu-

lar field constant depending on $T_C$, then one has $B(T)=\lambda \cdot M(T)$. The temperature dependence of $M_{\mathrm{sat}}(T)$ has to be determined numerically using the complete Brillouin function.

The thermal occupation of the $i$th $M_J$ state of the atom is given by

$$n_i(T)=\frac{\exp\left\{\frac{U_i}{k_BT}\right\}}{\Sigma \exp\left\{\frac{U_i}{k_BT}\right\}}, \tag{9}$$

where the sum has to be taken over all $M_J$ states according to $-J \leqslant M_J \leqslant J$, $U_i=M_J g \mu_B B(T)$, $g$ is the Landé factor or gyromagnetic ratio, and $\mu_B$ is the Bohr magneton. At $T=0$ only the state with $M_J=-J$ is occupied, whereas at $T=T_C$ and above all $M_J$ substates are equally distributed. (We have neglected the presence of short-range magnetic order for $T>T_C$, as appropriate to a molecular field model, although actually studying such short-range order via MCDAD measurements would be interesting in the future.) From the occupation of the $M_J$ states with temperature, we derive the contribution of the single-particle $m_j$ states needed to calculate the photoemission amplitudes. Figure 3 shows the thermal occupation $n_{M_J}$ of the $M_J$ states for the ${}^8S_{7/2}$ ground state together with the resulting single-particle partition numbers $n_{m_j}(T)$ for the ${}^9D_6$ line as calculated numerically. (Note that for $\underline{J}=6$ only the state with $j=\frac{5}{2}$ contributes.) All other lines follow the ground state $M_J$ occupation in a similar way but with varying contribution of the single electron $m_j$ substates. These partition numbers now take account of the varying population of the initial state multiplet. The sum of the partition numbers is constant over the entire temperature range. The $|\frac{5}{2},-\frac{5}{2}\rangle$ state is the dominating single-particle state for the $\underline{J}=6$ line. It is interesting to note that the $|\frac{5}{2},-\frac{3}{2}\rangle$ state has a slight maximum in the partition numbers at about $T=0.63T_C$. From the temperature dependence of the $M_J$ or $m_j$ states it follows that orientation and alignment of the initial and possible final states (as allowed by the selection rules) become temperature dependent, too.

The intensities of the $\underline{J}=1-6$ lines of the multiplet have been calculated for excitation with RCP and LCP light by varying the sample orientation and magnetization together over $\Phi_M=0-360°$ in steps of 2° for the geometry as shown in Fig. 1. $\Phi_M=0$ refers to the case for which the magnetization is in the incident photon plane.

The dichroic asymmetries for a particular state and photon helicity are calculated in two ways: from the intensities for two antiparallel orientations of the magnetization at fixed helicity (CMDAD) or from two intensities with opposite photon spin $\sigma$ at fixed magnetization (MCDAD) from

$$A_{\mathrm{CMDAD}}[\%]=100 \cdot \frac{I(\Phi_M)-I(\Phi_M+\pi)}{I(\Phi_M)+I(\Phi_M+\pi)},$$

$$A_{\mathrm{MCDAD}}[\%]=100 \cdot \frac{I(\sigma^+)-I(\sigma^-)}{I(\sigma^+)+I(\sigma^-)}. \tag{10}$$

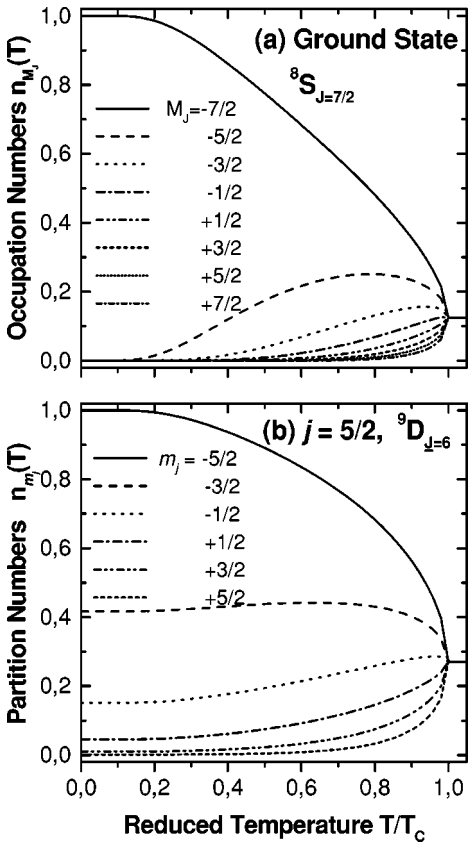


FIG. 3. Statistical multiplet parameter. (a) Temperature dependence of the $M_J$ occupation numbers for the ${}^8S_{7/2}$ ground state of remanently magnetized Gd. (b) Single electron $m_j$ partition numbers for transition from the ground state into the ${}^9D_6$ excited state by photoexcitation of $d_{5/2}$ electrons, with the Curie temperature assumed to be $T_C=292$ K.

## IV. RESULTS AND DISCUSSION

Figure 2(a) shows examples of Gd $4d$ core-level spectra taken with RCP light for two different orientations of the magnetization axis, here denoted as parallel ($p$=solid points and line) for the magnetization **M** maximally parallel to the incoming light **q** and antiparallel ($m$=open points and dotted line) for the magnetization direction being maximally opposite to the incoming light. One clearly sees a general splitting of the spectrum into what has been found to be primarily ${}^7D$ and ${}^9D$ states,[12] with the ${}^9D$ states at higher kinetic energy being resolved into further components. It should also be mentioned here that there are more multiplet states of ${}^7D$ symmetry at higher binding energies (lower kinetic energies) outside of the range of this spectrum, with some at more than 20 eV higher.[12] It should be noted that these satellite lines are much more pronounced at higher excitation energies of about 1 keV as reported in Refs. 73 and 74. For the purpose of the present study, however, we will concentrate on the binding energy range shown in Fig. 2. Also shown in Fig. 2(b) is a normalized magnetic dichroism difference spectrum obtained from these two spectra after subtracting a Shirley-type inelastic background.[75] In calculating this from the experimental data, we do not use the normally cited asymmetry as in

Eq. (10) but instead use a normalization to the maximum value of the sum of the two curves,

$$\chi_{\mathrm{CMDAD}}(E)[\%]=100\cdot\frac{I_p-I_m}{\max(I_p+I_m)}. \tag{11}$$

In this way we avoid having a very noisy signal in the wings of the core-level spectra due to division by small numbers, with additional complications at the high binding energy side due to the neglect of the multiplet states there. The value derived in this way also seems to coincide with the one derived by normalization to the total area under the dichroism curve. We will thus use the peak-to-peak value here for convenience. We have checked, however, that the results are not influenced by the choice of the normalization function. In addition, the spectra of Fig. 2(a) have been normalized by matching the integrated areas under the curves before calculating the difference, in order to account for small changes in the photon flux. This procedure assumes a vanishing integral of the dichroism, which is supported by the fact that these corrections of $\leqslant$10% are random in nature and do not introduce any new features. The final calculated asymmetry curve (here measured with fixed helicity) resolves the individual final states of the $^{7,9}D$ multiplet significantly better than the experimental results presented in a prior MCD study.[12] Our results as shown in Fig. 2 also agree very well with other high-resolution measurements of the Gd $4d$ core level that have been reported.[76] It should be mentioned here that the observed effect is in the range between $-15\%$ and $+35\%$, and this is remarkably high for measurements at room temperature.[77]

Calculations for the many-electron case according to the theory presented in the last section and for a temperature of 250 K are shown in Fig. 2(c) and they agree very well with the measured intensities and dichroism. It should be noted that the additional lines at lower energies are only observed in the calculations if the restriction on pure coupling schemes is lifted. Our calculations show, however, that some additional restriction to the ground state does not at all change the dichroism of the $^9D$ part of the multiplet. The present restriction of both the ground state and the intermediate ionic state reduces the number of lines drastically down to 30 [see Fig. 2(c)]. In **LS** coupling, the only final state (ion plus free electron) that can be reached from the $^8S$ ground state is $^8P$ according to the angular momentum selection rules for **LS** coupling conditions: $S'-S=0$ and $L'-L=0,\ \pm1$ $(L=L'\neq0)$. The spin is not changed because the dipole operator does not act on the spin and here the orbital angular momentum can be changed only from 0 to 1. In intermediate **LSJ** coupling the final angular momentum (again ion plus free electron) takes the values $J'=\frac{5}{2},\frac{7}{2},\frac{9}{2}$. The final states will be degenerate with respect to some particular $L'S'J'$ but this degeneracy is lifted with respect to the excited hole state $\underline{LSJ}$. The complete transition matrix may be found elsewhere.[64,65] For the excited hole state we have to couple the $^8S$ ground state of the seven equivalent $4f$ electrons to the hole in the $4d$ shell resulting in the $^{7,9}D_{\underline{J}}$ multiplet with overall ten states in **LS** or $\mathfrak{J}$**J** coupling. In addition, the coupling of the $4f$ electrons may also lead to the non-ground-state levels that are $^2(S\cdots Q)$, $^4(S\cdots N)$, and $^6(P\cdots I)$ where the dots "$\cdots$" assign all orbital angular momenta between the two limiting cases given in the brackets. Some of the states are reached via different parent and grandparent states and therefore one has overall 118 different **LS** states besides the ground state. On the other hand, the free electron has the orbital angular momentum $p$ or $f$ and we find the hole states $\underline{LS}\ ^{7,9}(S\cdots G)$ if uncoupling the free electrons from the overall final state $L'S'$. It is seen that the excited $^9D$ hole can only be reached from the $^8S$ ground state, whereas the $^7D$ hole can also be reached from the non-ground states $^6(PDFG)$. The assignment of the structures observed in Gd $4d$ photoemission is not unique through the literature.[12,78,79] In Ref. 12 the additional lines have been attributed to transitions including only the $^6(PDFG)$ states. However, in intermediate coupling $J$ is a good quantum number rather than only $LS$. This leads to some more allowed combinations and the most prominent additional states found in the calculated spectra are $^7(SPFG)_{\underline{J}}\ \underline{LSJ}$ core holes. Cowan's program allows easily restrictions to the initial $LS$ (first parity) and final $L'S'$ states (second parity) but not the easy selection of a collection of intermediate $\underline{LS}$ states. Moreover, a restriction to a particular initial or final state does not lead automatically to restrictions on the intermediate states. This may lead to situations where accidentally different sets of states are used for the initial and final states. In this work, we made a minor modification to the Cowan program to allow only the couplings that can be derived via the $^{7,9}D_{\underline{J}}$ core hole, but we account for all states of the intermediate coupling scheme. The $\mathfrak{J}$**J** or **jj** coupled pendants are derived from an unambiguous transformation matrix (see Ref. 64). It was carefully checked that the restrictions do not effect the overall behavior of the spectra and that the results fit the measurement. We note that the spectra so derived are in agreement with the ten levels observed from a full relativistic calculation; however, many-electron calculations without any restrictions will deliver some ten thousand lines. It is not meaningful to account for such lines in the present study, since most of the secondary excitations typical of solid-state electron spectroscopy (plasmon or interband transitions to name some of the most pronounced) are also neglected, and would act to smear over any effects due to this manifold of lines.

### A. Angular dependence of the dichroism

#### *1. Normal emission*

We now consider the angular dependence of the dichroism by taking pairs of spectra like the ones shown in Fig. 2(a) for different orientations of the sample. For each angle $\Phi_M$ we thus recorded the overall CMDAD value. Figure 4 shows part of an angular dependent measurement of the magnetic dichroism. Figure 4(a) shows the difference spectra for opposite magnetization $I_p-I_m=I(\Phi_M)-I(\Phi_M+\pi)$, that is, the CMDAD ($\Phi_M=0$ refers to the case where $M\|x$); (b) shows the sum of spectra taken with opposite magnetization and fixed helicity for some selected angles. As the absolute cross section is not known, we normalized all spectra in Fig. 4 to the same background level $I_0$ for energies above the highest line of the multiplet. This procedure allows at

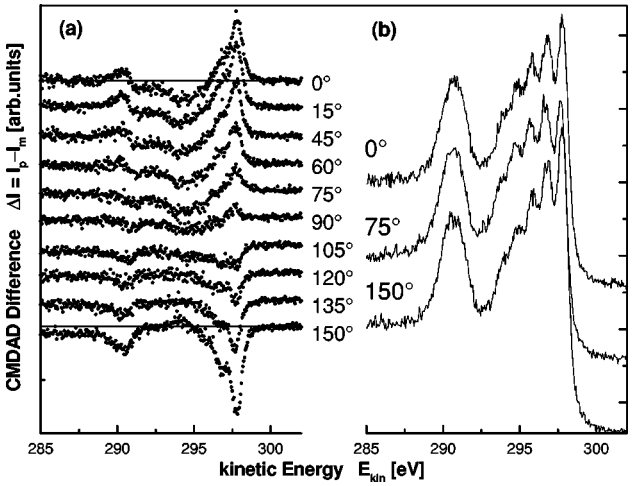


FIG. 4. Angular dependence of the magnetic dichroism for Gd $4d$ core-level. (a) Difference of spectra taken with opposite magnetization and fixed helicity. (b) Sum of spectra taken with opposite magnetization and fixed helicity. (Emission normal to the surface, with a photon energy of 438.9 eV, an angle $\alpha=70°$ and $\sigma+$ polarization. $\Phi_M=0$ refers to the case where the magnetization is in the incident photon plane and parallel to the $x$ axis; at $\Phi_M=90°$ magnetization and photon propagation are perpendicular to each other, see also Fig. 1.)

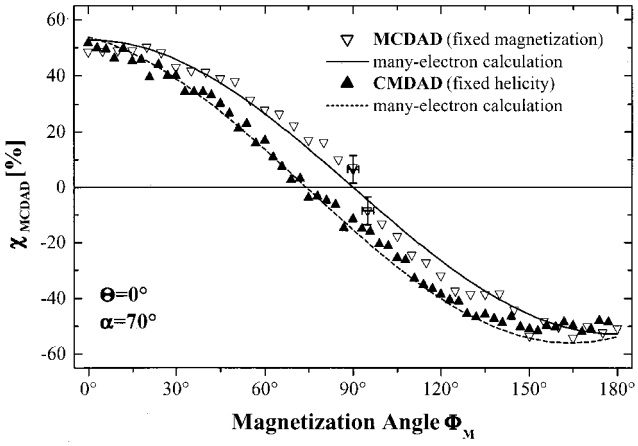


FIG. 5. Angular dependence of the overall dichroism for Gd $4d$ core-level emission normal to the surface, with a photon energy of 438.9 eV and an angle $\alpha=70°$. Experimental results are shown for the fixed-magnetization mode with variable light polarization (MCDAD, open inverted triangles) and for the fixed-helicity mode with variable sample magnetization (CMDAD, solid upright triangles). The solid and dashed lines show theoretical curves calculated for the respective cases using the relativistic many-electron approach.

least a convenient comparison of the spectra. The sum spectra exhibit some small differences in the intensity ratio of the $J=5$ and $J=6$ lines of the $^9D$ part for different angles. The sum spectra correspond to an aligned ensemble and the photon beam is not completely circularly polarized. Therefore differences in sum spectra may reflect a remaining nonmagnetic LDAD while rotating the alignment of the ensemble. From the difference spectra it is seen that they tend to smear out the fineness of the multiplet structure. A convenient way for data analysis is the use of an overall dichroism $\chi$ from Eq. (11) defined above:

$$\chi_{\mathrm{CMDAD}}=\max[\chi(E)]-\min[\chi(E)]. \tag{12}$$

This makes an estimate of the dichroism possible without using any sophisticated fitting procedures. It may be seen, however, that the dichroism is dominated by the $J=6$ line, rather independent of the angle. The resulting data set for normal emission is summarized by solid triangles in Fig. 5, where we plot the overall CMDAD as a function of $\Phi_M$.

The data in Fig. 5 basically exhibit a cosinelike behavior which would be expected from the free-atom case.[9,11,58] Our theoretical simulations (relativistic many-electron approach) yielding the dashed curve are in excellent agreement with the measurements. Note that the zero crossing of the CMDAD does not occur at a rotation angle of 90° where magnetization and photon propagation are perpendicular to each other, but rather close to 72°. This shift in the zero crossing is very well predicted by theory, as shown by the dashed curve in Fig. 5. Its cause will be discussed in detail after showing the data for the circular dichroism.

So far the dichroism reported has been derived from measurements performed by changing the magnetization direction relative to the light polarization (as noted above, we will call this the CMDAD or fixed-helicity mode in what follows). We have the situation of CDAD measurements if switching the light polarization from RCP to LCP for each (fixed) angle of magnetization $\Phi_M$ which will be called MCDAD or fixed-magnetization mode. The difference and sum spectra look similar to those of the CMDAD case shown in Fig. 4 and we accordingly do not reproduce them here. We obtain the result shown by open triangles in Fig. 5 when using the overall MCDAD value calculated in the same way as for CMDAD in Eqs. (11) and (12) and Fig. 2.

We still observe a fairly smooth variation with angle $\Phi_M$, making it clear that the MCDAD in this mode is not scattering induced, but now the zero of the dichroism occurs very close to 90°. The small step around 90° marks the noise level in our data which makes it impossible to detect zero to better than about 5%. This can be seen from the difference spectra taken at $\Phi_M$ of 90° and 105° [in Fig. 4(a)], showing that the change of sign of $\chi$ cannot be determined very well at low level. In addition one recognizes some influence from the asymmetric line shapes. However, the step is more pronounced in the MCDAD data compared to the CMDAD data. This is most probably due to a small misalignment of the sample resulting in a nonmagnetic CDAD.

Our theoretical simulations for the MCDAD yield the solid curve, again in very good agreement with the measurements. It is thus clear that care is needed in making what is often the experimentally simpler type of fixed-helicity CMDAD measurement, as it may differ significantly (here by up to 10% in overall magnitude) from the fixed-magnetization MCDAD measurement.

Comparing both measurements it clearly follows that the magnetic (fixed-helicity) and the circular (fixed-magnetization) dichroism are different if the magnetization is not parallel to the plane of photon incidence. This behavior

may be easily explained. The dichroism in angular resolved measurements using circular polarized photons depends not only on the orientation $\rho_{10}$ but also on the alignment $\rho_{20}$ of the electronic states. This can be found easily from the general equations given by Klar and Kleinpoppen[80] or from the work on *p* states of Cherepkov *et al.*[10] For *d* states one will have additionally higher moments ($\rho_{30}$ and $\rho_{40}$) that contribute to the dichroism. The so called state multipoles $\rho_{N0} = \rho_{N0}(j,m_j)$ are defined in the textbook of Blum.[81] The orientation-dependent (odd *N*) term is clearly connected with the magnetic dichroism, whereas the alignment-dependent term (even *N*) of the MCDAD may already be observed without magnetization (CDAD case). Unfortunately in the magnetized case, orientation and alignment of the states cannot be separated easily. The alignment dependent terms of the CDAD vanish in every nonchiral symmetry. This may occur in the present case when the plane of photon incidence coincides with the plane of magnetization. Now, if the magnetization is rotated in the surface plane, one may find situations of chiral symmetry, that is state alignment, and photon incidence, and angle of observation are co-planar. On the other hand if we change the magnetization between two antiparallel directions, only the orientation of the states is changed, but not their alignment. The result is that the intensities for these two cases may depend only on the orientation of the states. It immediately follows that the fixed-helicity mode (CMDAD) and fixed-magnetization mode (MCDAD) are only the same in a nonchiral geometry.

We will now use the single electron approach to express this more quantitatively. Consider a single electron *d* state ($l=2$) with total angular momentum $j=l\pm\frac{1}{2}$. Using the single electron approach, we find that for given *j* and a particular value of $m_j$ the MCDAD (here the difference of the spectra and not the asymmetry) in dependence of the direction $\Phi_M$ of magnetization is given by

$$\begin{aligned} I_{\mathrm{MCDAD}} &= \rho_{10}C_{11}\cos(\Phi_M) + \rho_{20}C_{21}\sin(2\Phi_M) \\ &+ \rho_{30}[C_{30} + C_{32}\cos^2(\Phi_M)]\cos(\Phi_M) \\ &+ \rho_{40}[C_{40} + C_{42}\cos^2(\Phi_M)]\sin(2\Phi_M). \end{aligned} \quad (13)$$

Here we assumed in-plane magnetization, off-normal incidence and emission. The coefficients $C_{ij}=C_{ij}\ (R,\delta,\mathbf{q},\mathbf{k})$ depend on the dynamical parameters *R*, $\delta$ (reflecting the interference of the final-state partial waves). They also depend on the directions of photon incidence **q** and electron emission **k**. The terms connected to $\rho_{N0}$ with $N>2$ contribute only for $d_{5/2}$ states to the MCDAD, but not for $d_{3/2}$. It should also be noted that the MCDAD for the $d_{3/2,\pm 1/2}$ states vanishes for the case that photon incidence and magnetization are in one plane and the electron emission is in a direction perpendicular to that plane if the final-state spin orbit interaction is neglected. But, it is nonzero under these conditions for all other *d* states.

In a similar way we find that the $\Phi_M$ dependence of the CMDAD is given by

$$\begin{aligned} I_{\mathrm{CMDAD}} &= \rho_{10}[C_{11}\cos(\Phi_M) + C_{12}\sin(\Phi_M)] \\ &+ \rho_{30}[C_{31}\cos(\Phi_M) + C_{32}\sin(\Phi_M) \\ &+ \cdots + C_{33}\cos(\Phi_M)\sin(2\Phi_M) \\ &+ \cdots + C_{34}\cos^3(\Phi_M)]. \end{aligned} \quad (14)$$

The CMDAD does not contain $\rho_{N0}$ terms with even *N*. This expresses directly the different role of the alignment of the states on the type of dichroism, as explained above. The coefficients $C_{ij}$ differ in general from those describing the MCDAD. It is directly seen that the MCDAD becomes always zero for $\Phi_M=90°$, whereas the CMDAD remains if the coefficients connected to the $\sin(\Phi_M)$ terms do not vanish, what is the case in a general geometry. This explains directly the observed shift of the zero crossing between the two methods.

Analyzing the dependency of the coefficients with respect to the dynamical parameter, we find that the shift of the zero crossing is caused by interference between the *p* and *f* outgoing photoemission channels, and is not the result of photoelectron diffraction, as noted previously.[58] The cross channel interference between the $j_f=j_i$ and $j_f=j_i+1$ channels,[7] or additionally with the $j_f=j_i-1$ channel[82] (for initial states with $j_i>\frac{1}{2}$), can in addition induce spin polarization independent of a magnetization if circularly polarized light is used for the excitation. The second case shows that, for $l_i>0$, the cross-channel interference between the $l_f=l_i\pm 1$ channels is the main cause of the spin polarization due to the presence of spin-orbit splitting in the initial state.

As this approach is valid for all single electron $m_j$ substates, we will also find the same result for the multiplet approach, in agreement with the work of Thole and van der Laan.[9] The $\Phi_M$ dependence of the overall asymmetry will have a slightly different shape compared to Eqs. (13) and (14), but this is caused by the normalization and not a direct effect of the multiplet nature of the lines.

#### *2. Off-normal emission*

We turn now to off-normal emission directions, in particular to $\Theta=20°$ off-normal where the photoelectron momentum **k** is normal to the photon propagation **q**. For this case, we might expect enhanced photoelectron diffraction effects due to the rotation of the emission direction through various scatterers in the near-surface region. We consider the case where the magnetization direction is reversed with fixed helicity of the photons (RCP). The experimental results are shown as solid squares in Fig. 6. Here one notices some distinct deviations from the smooth free-atom behavior, and these are reproducible over various sample preparations studied. The additional modulations in the CMDAD values riding on the overall cosinelike curve are of about $\pm 5\%$ and are due to photoelectron diffraction.

This becomes clear by comparing the experimental results with the result of our photoelectron diffraction calculations as carried out at two temperatures, $T=250$ K as in the experiment and 0 K for comparison with free-atom models. Most of the main peaks and valleys in the experiment are at

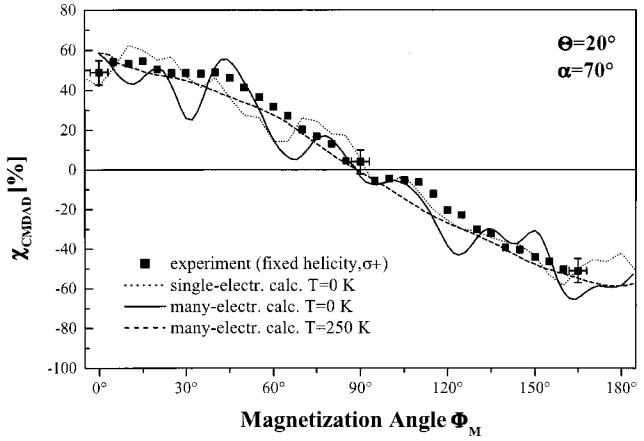


FIG. 6. Azimuthal dependence of the overall CMDAD for Gd $4d$ core-level emission at an emission angle 20° away from the normal direction, again with a photon energy of $h\nu = 438.9$ eV and $\alpha = 70°$ photon incidence. The squares represent typical experimental data, and the lines show theoretical calculations for this geometry. The solid line is for the relativistic many-electron calculation with a temperature of 0 K, whereas the dashed line represents the analogous results for $T = 250$ K. The dotted line shows results of the single electron calculation.

least qualitatively reproduced by the many-electron theoretical curve at 0 K, although theory shows more exaggerated diffraction features than experiment. The analogous many-electron curve at 250 K seems to suppress diffraction too much, perhaps due to oversimplifications in the Debye-Waller factor approach, which neglects vibrational correlation among near-neighbor atoms. Using the simpler single electron picture with multiple scattering and at 0 K (dotted curve) is found to roughly agree with experiment and many-electron theory at the same temperature. The obvious angular shift between the experimental and calculated wiggles is most probably due to a slight misalignment of the sample; however, we will come back to that point later when discussing the state resolved results. Here we just remark that experiment and theory show both some influence of photoelectron diffraction. The result of *ab initio* calculations is for both types in the correct order of magnitude but needs some refinement to include experimental uncertainties.

These differences should also illustrate the potential one still has in tuning different parameters so as to get better agreement between theory and experiment. It should also be pointed out that the positions of the main features do not coincide with forward-scattering maxima, which should occur at intervals of 60°. Based on data not shown here, the $\Phi_M$ dependence for this emission angle also is found to depend on the way the dichroism is measured (fixed-helicity or fixed-magnetization direction mode); however, the dependence is much weaker than in the normal emission case. In particular, we do not observe a shift of the position of the zero dichroism between the two modes, because photon incidence and electron ejection are perpendicular to each other: $\alpha + \Theta = 90°$. In that case the coefficients $C_{12}$ and $C_{32}$ in Eq. (14) vanish. If one compares the normal and off-normal emission experiments with each other (both measured in fixed-helicity mode) it is clear that one observes, besides the introduction of the diffraction features, the shift of the zero CMDAD position from 70° back to about 90° for the off-normal emission case where photon incidence and electron ejection are perpendicular to each other.

The additional scattering-induced oscillations in the dichroism clearly depend on how the experiment is performed. The calculations show that they appear only in the case where both the sample and the magnetization are rotated together. The case of pure magnetic dichroism, that is, the case where only the magnetization is rotated while keeping the sample orientation fixed, results in a smooth atomiclike behavior of the dichroism as in normal emission. This situation, however, can hardly be realized in experiments where the magnetization is usually determined by various so-called *easy* directions.

In terms of diffraction-induced CDAD, we might in principle expect to observe a peak ''rotation'' of the total intensity maxima in switching from LCP to RCP light, as discussed by Daimon *et al.* for Si(001),[15] and subsequently observed for W(110) and adsorbates.[16–18] In results not shown here, we have plotted the total intensities for LCP and RCP light as obtained from the theoretical calculations (in fixed-magnetization direction mode) for the geometry considered here, and we observe a fairly substantial shift of the diffraction maxima by about $\pm 10°$; however, for our experimental data we are unable to see this effect clearly. This is due to the small intensity variations with angle for these directions which are not at all forward-scattering directions. Additionally, problems with the absolute normalization of LCP and RCP only allowed a comparison between intensities measured with linear-polarized light with those measured with RCP light. In this case, we do see a small shift of the apparent features that is qualitatively consistent with peak rotation. More precise future measurements would be needed to clearly resolve such peak rotation effects, however.

Finally, by making use of the relatively high resolution of our spectra, we can also fit the separate states in the $^9D$ part of the Gd $4d$ core-level spectrum. Using the same equation for the CMDAD for each individual state then gives us a state-specific CMDAD. In Fig. 7(a) we have plotted this value for the first five states ($^9D_{J=6-2}$) as a function of magnetization azimuthal angle $\Phi_M$ for the off-normal emission case. The intensity for the $J=1$ line could not be extracted from the data unambiguously. It is clear that the states contribute differently to the overall behavior of the CMDAD. In particular the dichroism is positive for the $J=6,5$ lines whereas it is negative for the remaining part of the $^9D$ core hole. Furthermore, there are different angular dependencies for the different states. The difference in the kinetic energy between the observed lines is too small to explain the different angular variations by scattering effects alone. These differences are directly attributed to the different emission characteristics of the single-particle states contributing to the lines.

We will now analyze the state-specific dichroism with the two different theoretical models (single electron, multiple scattering versus many-electron, single scattering). We show in Fig. 7(b) the CMDAD calculated in the nonrelativistic single electron multiple-scattering model for the six $m_j$ states

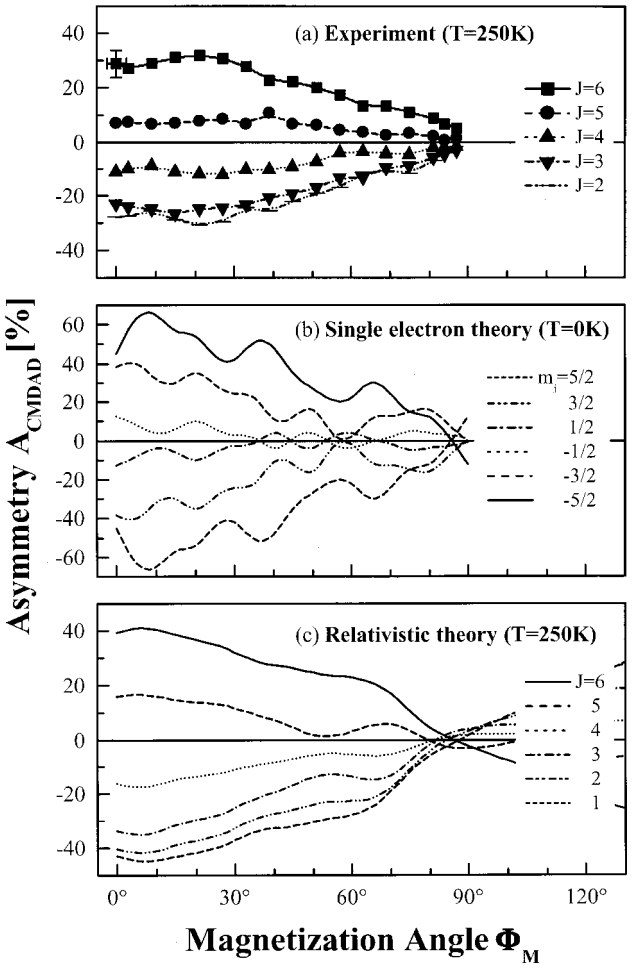


FIG. 7. State-specific Gd 4*d* CMDAD. Measured CMDAD asymmetry for the first five states of the $^9D$ part of the Gd 4*d* core-level spectrum as shown in Fig. 2(a). The intensities have been derived from high-resolution spectra by using a curve fitting procedure (Voigt-type peaks plus Shirley-type background). The CMDAD asymmetry was calculated from Eq. (10). (a) Experimentally derived state-specific CMDAD at $T=250$ K. (b) Simulated state-specific CMDAD, for the six $m_j$ states in the $j=\frac{5}{2}$ manifold in the nonrelativistic single electron model including multiple scattering. (c) Simulated state-specific CMDAD, calculated using a full relativistic, final-state multiplet description yielding the *J* states of the $^9D$ part of the Gd 4*d* core-level spectrum. The $J=1$ line arising in **jj** or intermediate coupling is shown for completeness.

of the $j=\frac{5}{2}$ initial state, although recognizing that these states certainly do not map directly onto the different *J* states of the $^9D$ manifold. Each of these states contributes in a different way to the dichroism of the individual *J* lines. For example, the $m_j=-\frac{5}{2}$ dominates the $J=6$ line as can be seen from Fig. 3. It exhibits three pronounced scattering induced features, similar to the experimental data, but at different angles. That these features are indeed induced by scattering can be found from a pure atomic calculation as is shown in Fig. 8, where we compare circular and magnetic dichroism for the single and many electron states. It is clearly seen that circular and magnetic dichroism are much different for the single electron states, but both asymmetries are much smoother than those including scattering. The additional alignment terms ($\rho_{20}$ and $\rho_{40}$) of the CDAD cause additional zero crossings for some of the single electron states. It is interesting to note that both methods come closer to each other in the many electron description, what is caused by its averaging character. It is also shown that the scattering together with the mixing of the single-particle states smears out the zero crossing that is found to occur at 90° in the pure atomic calculation, independent of the states; however, the scattering induced features in Fig. 7(b) are too strong and do not coincide with the measured structures. Therefore we will use the full relativistic simulation for further comparison, as the single electron approach alone cannot be brought into closer comparison with the measured CMDAD, as might be expected.

The more sophisticated full relativistic simulations of the state-specific dichroism in terms of final-state multiplets are shown in Fig. 7(c). This calculation results in all six *J* states for comparison to the five resolvable in experiment, and it shows angular variations for all five which are very similar to the measured data. The calculations also reproduce correctly the sign and magnitude of the measured CMDAD. The slight difference in magnitudes between theory and experiment could be due to our allowance for thermal effects using the molecular-field approach. The scattering induced features are smaller compared to the single electron approach. This is not caused by the mixing of the states but by the inclusion of thermal effects in the scattering formalism (Debye-Waller). These features do not coincide very well with the experimental ones and additionally there is a small shift between the observed and the calculated zero crossing of the CMDAD ($\approx$90° and $\approx$85°, respectively). Both facts hint on a small misalignment of the sample with respect to the nominal geometry. All of the previously shown calculations have been done *ab initio* and were all performed for the nominal geometry of the experiment. Therefore we finally tried to change the geometry of the calculations in order to find a better agreement.

For better comparison, we show in Fig. 9 the difference between the smooth atomic curves and the measured or calculated magnetic dichroism. This difference provides a measure of the scattering induced dichroism. We selected the $J=6$ state for the comparison, because the experimentally determined dichroism is less depending on the fitting procedure as compared to the other *J* lines. The experimental data were oversmoothed and fitted to a cos series in order to determine the atomic like part. This fit was also used to find an angular offset of about $\Delta\Phi_M=7°$ being also used in the calculation. For the theoretical curve we subtracted directly the results of an atomic calculation by switching off the scattering part. The oscillations in the experiment are about $\pm 3\%$, whereas the calculation shows differences ranging from $-12\%$ to $+4\%$. It may be seen in Fig. 9(a) that the calculated dichroism at $\Phi_M=0$ is about 40% but only 30% in the experiment. The calculated value is too high, which suggests either a deviation in the used *ab initio* dynamical parameter or a lower degree of polarization in the experiment. The local minima and maxima of the difference curves shown in Fig. 9(b) exhibit the same behavior in experiment and calculation.

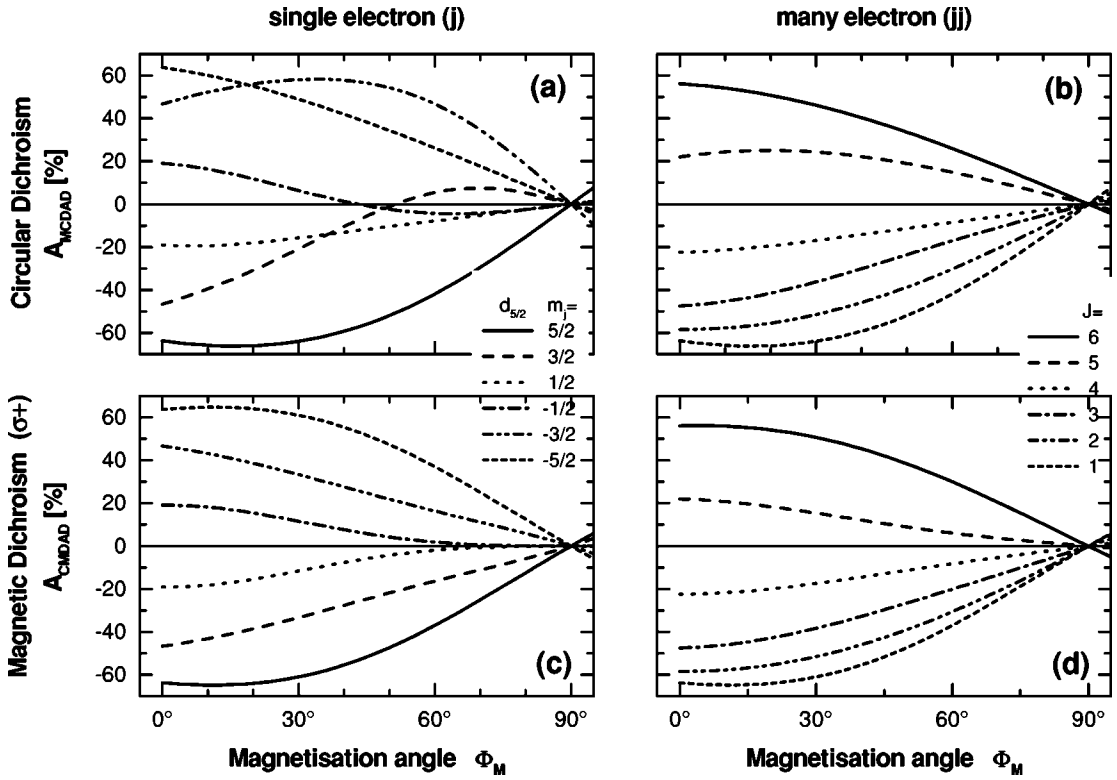


FIG. 8. Atomic part of the Gd 4*d* dichroism in off-normal emission. Top row: Circular dichroism. Part (a) shows the MCDAD in single electron description and part (b) shows the MCDAD in **jj** coupling. Bottom row: Magnetic dichroism. Part (c) shows the CMDAD in single electron description and part (d) shows the CMDAD in **jj** coupling. (Parameters are $T=0$ K, for photons $h\nu=450$ eV, $\alpha=70°$ and for electrons $\Theta=20°$, $\Phi=\pi$.)

Deviations are mainly due to the angular acceptance of the spectrometer, that smears the features out by integrating over a certain angular range. On the scale of the data presented here, one may thus consider the many-electron single-scattering description to be very accurate.

### B. Temperature dependence of the dichroism

The dichroic signal also provides a measure of the magnetization of a particular sample, but only indirectly as will be shown below. For example, a nonzero MCDAD implies a nonzero magnetization and a zero MCDAD for a direction initially showing a nonzero effect also implies a zero magnetization; however, if a direction initially showing zero effect is studied, there may be no sensitivity to a loss of magnetic order. Thus, with proper choice of geometry, following to measurements of the MCDAD signal as a function of temperature should permit monitoring of the transition behavior and the magnetic transition temperature.

In the present case, we started with the sample cooled down to about 250 K and measured again pairs of spectra for two sets of data, that is, for opposite magnetization directions or opposite light helicity, respectively. Since the change in magnetization as a function of temperature should be independent of the emission angle, we chose a geometry with maximum signal. In this particular geometry (normal emission, $\Phi_M=0$) the results do not depend on the measurement mode, and we show MCDAD data taken in the fixed-magnetization mode. From these spectra we get the overall MCDAD value as described before, and these are plotted in Fig. 10 as a function of the sample temperature. The sample temperature was measured indirectly by taking the temperature at a cold finger which touches the sample.[41] The temperature scale in Fig. 10(a) was finally derived from a calibration of this reading with a thermocouple directly touching the sample surface. This procedure is rather delicate, especially in the case where the sample is rotated to change the magnetization axis, and therefore the temperature measurements may have a systematic error of the order of $\pm 5$ K.

From Fig. 10 one sees that the MCDAD signal decreases with increasing temperature so as to reach approximately zero at a temperature close to the Curie temperature for films of this thickness. For the highest temperatures, there is approximately a 5% asymmetry offset from zero. This offset may arise as follows: First, a slight orientational misalignment can lead to a diffraction induced MCDAD even above the Curie temperature. Second, differences in the intensities may occur with polarization when switching from the beam above to below the storage ring plane, due to the different optical paths taken. Finally, the grazing incidence setup of the monochromator may lead to a small linear polarization that changes sign if the helicity of the initial photons from the storage ring is switched, leading to an additional LDAD, as reported previously;[83] however, the observed offset is also of the order of the noise level (as described above) and does not affect our discussion of the physics behind the temperature dependence.

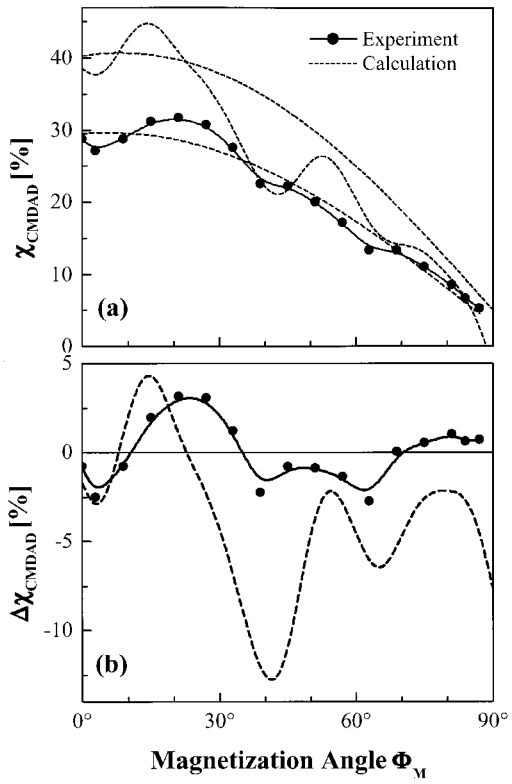


FIG. 9. Scattering induced dichroism in Gd 4*d* off-normal emission. (a) Comparison of the measured and calculated CMDAD of the $^9D_6$ state from Fig. 7 after correction of $\Phi_M$ (as assigned by the experimental value) in the calculation by 7° at $T=250$ K (dashed lines represent the atomic like part). (b) Difference of the CMDAD after subtracting the atomic like part (for details see text).

In order to illustrate the temperature dependence of the MCDAD we have included in Fig. 10 magneto-optical Kerr effect (MOKE) measurements from Gd films of comparable thickness (30 nm) of Farle and Lewis[51] as well as measurements of the exchange splitting ($\Delta E_{\mathrm{Exc}}$) of the surface state by Weschke *et al.*[39] found from photoemission and inverse photoemission experiments [8 nm on W(110)]. The MOKE experiments are expected to be more bulk sensitive than the photoemission results or the exchange splitting of the surface state. The latter are directly correlated to the magnetic state of the surface. The MOKE curve indeed goes very close to zero as temperature reaches the bulk Curie temperature of Gd films, whereas $\Delta E_{\mathrm{Exc}}$ reaches zero at a noticeably elevated temperature. In this context it should be noted that spin resolved inverse photoemission [10-nm film thickness on W(110)] did not exhibit an enhanced surface transition temperature. This was attributed to possible different morphologies in different films.[84]

There is, however, a variation of the apparent transition temperature in the MCDAD data related to the cleanliness of the sample. For samples measured directly after the growth process the transition temperature seems to be ≈20 K higher than for the contaminated samples (taken up to 10 h after the growth). The latter samples were oxygen contaminated, mainly from residual gas adsorption, as found from the XPS measurements. Indeed, this is not a controlled adsorption experiment but results obviously in a change of the quality of the surface. However, it is well known that oxygen alters the magnetic properties of the Gd(0001) surface.[85] It should be noted that the elevated temperature for the zero of the MCDAD was observable up to 5 h after preparing the Gd layer. Well defined Gd(0001) tends to adsorb less oxygen, which highlights the high quality of the layer.

It is thus most probable that the elevation of the transition temperature for the clean surface is associated with the previously observed higher surface Curie temperature for Gd(0001),[36,38–41] an effect which has recently been suggested to be due to interlayer relaxation at the clean Gd(0001) surface.[42] From the previously reported results for Gd using spin-polarized low-energy electron diffraction (SPLEED),[36] one would in fact expect behavior such as we observe, rather than a residual low-level signal above the bulk Curie temperature as seen in the more bulk-sensitive MOKE measurements; however, further measurements with more carefully controlled surface cleanliness would be necessary to confirm this interpretation of our results.

Finally, we address the important question of how the dichroism is related to the temperature dependence of the saturation magnetization, at least in the molecular-field approximation. We therefore compare in Fig. 10(b) the magnetization as derived from the molecular-field approximation and the calculated normalized MCDAD of the $^9D_6$ multiplet state with the MOKE and MCDAD experiments as an illustrative case. After re-scaling the MOKE experiments fit very well to the saturation magnetization derived in the molecular-field approach. Nevertheless, there are small deviations close to the Curie temperature, that is, close to the phase transition. The measured overall MCDAD has also to be re-scaled (after subtracting the above $T_C$ asymmetry offset of about 5%) in order to fit the asymmetry calculated for the $J=6$ multiplet line. It is worth noting that the MCDAD reflects the average orientation of the atoms and therefore its temperature dependence should be very similar for the overall value and the most dominating line of the multiplet. The MCDAD from the O contaminated surface, and such reflecting more the bulk behavior, comes close to the calculated MCDAD. Nevertheless, deviations are seen close to the transition temperature as was also seen in the MOKE measurements. Possibly some surface magnetization is remaining above the bulk $T_C$ even at the contaminated surface.

From the comparison of the calculations (saturation magnetization and MCDAD) as well as the different experiments one clearly sees that the dichroism is not strictly proportional to the magnetization, but remains higher and then changes faster as the temperature comes closer to $T_C$. This is seen easily even though the $T=0$ asymmetry does not reach 100% as the magnetization saturates. Of course, the molecular-field model may be oversimplified, but even if short-range order were present, one might expect the dichroism to remain even higher as $T_C$ is approached. More quantitative future studies of this aspect would also be interesting.

These data thus represent a demonstration of the ability of temperature-scanned dichroism in core photoemission to detect the temperature variation of the magnetization as well as the ferromagnetic-to-paramagnetic transition. Future applica-

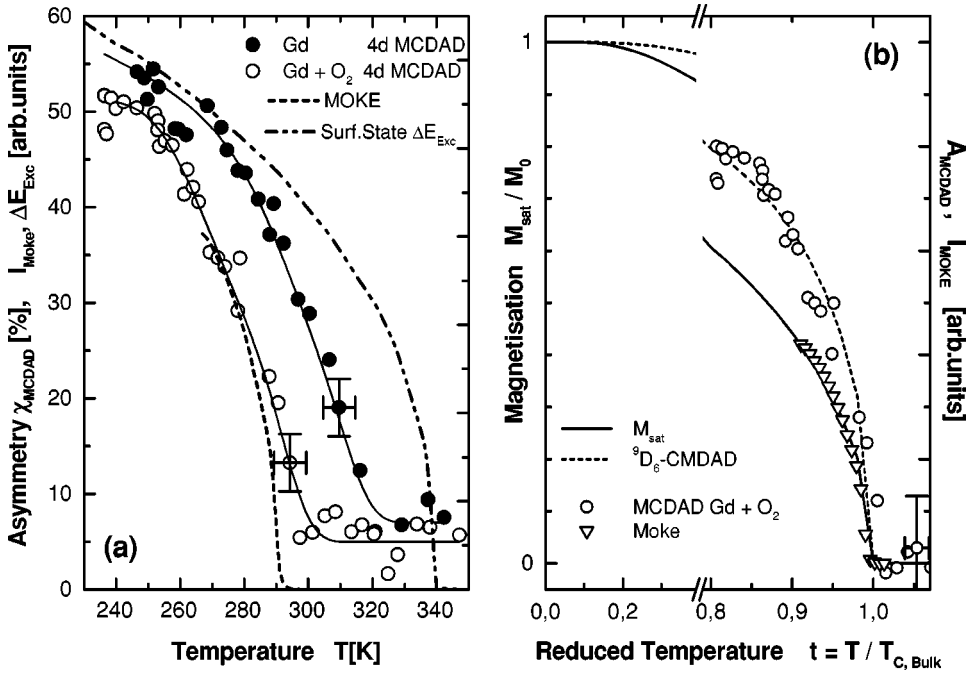


FIG. 10. Temperature dependence of the Gd 4*d* dichroism. (a) The overall MCDAD as obtained from 4*d* emission from Gd(0001) at a kinetic energy of about 295 eV as a function of sample temperature. Shown are two experimental curves for different sample conditions: fresh surface (filled squares), and an oxygen contaminated surface after ≈10 h in UHV (open triangles). The samples had a thickness of 28.7 nm and were annealed to 700 K. MOKE measurements (Ref. 51) from similar films of 30 nm thickness (dashed curves) and the exchange splitting $\Delta E_{\mathrm{Exc}}$ of the surface state (Ref. 39) (dash-dot) are shown for comparison. (The solid lines through the MCDAD data are simply guides to the eye.) (b) Temperature dependence of the saturation magnetization and the magnetic dichroism of the $^9D_6$ state calculated for a single magnetic domain of Gd and using the molecular-field model described in the text. The temperature is given on a reduced scale with the Curie temperature being assumed to be $T_C = 292$ K. The MOKE data of Ref. 51 (open triangles) and the MCDAD data of the contaminated sample (open circles) are shown for comparison. (All data have been re-scaled to be in the same order as the calculated saturation magnetization or MCDAD, see text.)

tions of this type seem to be very promising. Using measurements in fixed-helicity mode or in fixed-magnetization mode is found to yield the same results if the correct geometry is chosen carefully. In principle one could also consider using magnetic dichroism excited by linear or unpolarized photons to measure the same temperature dependency. In this case one should bear in mind that these types of dichroism might have a different dependency on the magnetization than the MCDAD, because different states are involved; however, in order to detect the transition temperature either or both methods could be used.

## V. CONCLUSIONS

For thick (≈100 ML's) Gd(0001) films grown on W(110), we have measured magnetic circular dichroism in the angular distribution of Gd 4*d* photoelectrons using two different approaches (fixed magnetization or MCDAD and fixed helicity or CMDAD), with effects as large as ±50% being observed. We have also modeled these effects using two approaches: a single electron multiple-scattering photoelectron diffraction theory, including spin-orbit and exchange interactions as perturbations only in the initial states, and a full-relativistic many-electron calculation to deal with the multiplet structure, plus spin-dependent single scattering with allowance for the magnetization of the sample as well as the full crystalline symmetry in the scattering potential. For 4*d* emission in the normal direction, we find that cross-channel interference between the two allowed *p* and *f* final states has a major influence on the angular behavior, which is very smooth and cosinelike in its azimuthal variation. Measurement of the MCD angular dependence with fixed magnetization and switching the photon polarization (MCDAD) is found to yield different results from measurement with fixed light helicity and rotation of the sample magnetization by 180° (CMDAD), indicating that care is needed in using the often-simpler second approach. For off-normal emission, our 4*d* data also reveal modulations superimposed on the smooth-curve behavior of about ±5% which are verified by comparison with the calculations to be due to photoelectron diffraction effects beyond the atomic model. The similarity between the results of both calculations as integrated over multiplet structure provide justification for using the simpler single electron picture to calculate properties of the multiplet as a whole, for which the more exact calculation would need much computation time. By contrast, our many-electron approach is necessary to describe quantitatively the CMDAD results as resolved for each peak in a multiplet. The correct inclusion of temperature effects (Debye-Waller and initial-state thermal populations) is also found to be important for a quantitative description.

The above findings are important in future uses of

MCDAD in order to derive magnetic properties, since the magnitude of the effect varies with both the geometry of the measurement (thus being sensitive to any change in the orientation of magnetization or short-range magnetic order; e.g., as a function of temperature), as well as emission direction (thus requiring allowance for additional diffraction effects in analyzing data and applying any sort of sum rule). In these respects, using such MCDAD in photoemission is more demanding than using x-ray-absorption MCD (XMCD), which is inherently angle integrating and which thus minimizes such effects. On the other hand, MCDAD is often a larger percent effect precisely because it does not angle integrate, and it has the further advantage of permitting more precise state-specific MCDAD measurements, such as we have demonstrated here for Gd 4*d* emission. Finally, we have demonstrated with the temperature-scanned data of this type that, with a high-brightness third-generation source for excitation and a high-luminosity electron analyzer, spectra can be accumulated rapidly enough to follow near-surface magnetic phase transitions via MCDAD in core photoemission. These results provide some further evidence for an elevated surface Curie temperature on Gd(0001) and, with future improvements in both data acquisition speed and temperature determination, this type of measurement should provide a further probe of surface and shallow-interface magnetism.

## ACKNOWLEDGMENTS

We would like to thank S. Rice for help with the experimental setup and E. J. Moler for help with the beamline. We also thank E. Kisker and M. A. Van Hove for fruitful discussions. We thank J. Braun (Universität Münster, Germany) for providing his ''Dirac-solver'' and the Gd solid-state potential. The authors are grateful to all members of the ALS staff for support during various beam-times. G.H.F. thanks Academia Sinica (Taipei, Taiwan) for the support extended to him during the final stage of this work. This work was financially supported by DOE, OER, BES, Mat. Sci. Div. (Contract DE-AC03-76SF00098), ONR (Contract N00014-94-1-0162), CNPq (202501/91-4, Brazil), DAAD/PROBAL (Contract 415-bra-probal/bu), NSC of Taiwan (Contract 89-2811-M-001-0002), and DFG (De 574/2-1, Germany).

*Also at Department of Physics, University of California Davis, Davis, CA 95616.

†Present address: Department of Physical and Theoretical Chemistry, University of Erlangen, Egerlandstr. 3, D-91058 Erlangen, Germany.

‡Present address: Universidade Federal do Rio Grande Do Sul, Inst. de Fisica, Porto Alegre 91501-970, RS, Brazil.

§Present address: Intel Corp., Materials and Technology Dept., Santa Clara, CA.

‖Also at Department of Physics, University of California Berkeley, Berkeley, CA 94720.

¶Present address: Vestek Systems, 388 Market Street, Suite 700, San Francisco, CA 94111.

**Present address: Department of Physics, La Trobe University, Bundoora VIC 3083, Australia.

[1] L. Baumgarten, C. M. Schneider, H. Petersen, F. Schäfers, and J. Kirschner, Phys. Rev. Lett. **65**, 492 (1990).

[2] E. Arenholz, K. Starke, and G. Kaindl, J. Electron Spectrosc. Relat. Phenom. **76**, 183 (1995); K. Starke, Z. Hu, F. Hubinger, E. Navas, G. Kaindl, and G. van der Laan, Eur. Phys. J. B **12**, 171 (1999); E. Arenholz, K. Starke, G. Kaindl, and P. J. Jensen, Phys. Rev. Lett. **80**, 2221 (1998).

[3] G. Panaccione, F. Sirotti, and G. Rossi, J. Magn. Magn. Mater. **198-199**, 677 (1999); G. Panaccione, F. Sirotti, and G. Rossi, Solid State Commun. **113**, 373 (2000).

[4] P. D. Johnson, Y. Liu, Z. Xu, and D.-J. Huang, J. Electron Spectrosc. Relat. Phenom. **75**, 245 (1996).

[5] J. Stöhr, J. Electron Spectrosc. Relat. Phenom. **75**, 253 (1995), and references therein.

[6] G. van der Laan and B. T. Thole, Phys. Rev. B **53**, 14 458 (1996), and references therein.

[7] M. S. Lubell and W. Raith, Phys. Rev. Lett. **23**, 211 (1969).

[8] U. Fano, Phys. Rev. **178**, 131 (1969).

[9] B. T. Thole and G. van der Laan, Phys. Rev. B **44**, 12 424 (1991); G. van der Laan and B. T. Thole, *ibid.* **48**, 210 (1993); B. T. Thole and G. van der Laan, *ibid.* **49**, 9613 (1994); G. van der Laan and B. T. Thole, *ibid.* **52**, 15 355 (1995).

[10] N. A. Cherepkov, V. V. Kuznetsov, and V. A. Verbitskii, J. Phys. B **28**, 1221 (1995).

[11] G. van der Laan, Phys. Rev. B **51**, 240 (1995).

[12] G. van der Laan, E. Arenholz, E. Navas, A. Bauer, and G. Kaindl, Phys. Rev. B **53**, R5998 (1996).

[13] J. G. Menchero, Phys. Rev. B **57**, 993 (1998).

[14] C. Westphal, J. Bansmann, M. Getzlaff, and G. Schönhense, Phys. Rev. Lett. **63**, 151 (1989).

[15] H. Daimon, T. Nakatani, S. Imada, S. Suga, Y. Kagoshima, and T. Miyahara, Jpn. J. Appl. Phys., Part 2 **32**, L1480 (1993).

[16] C. Westphal, A. P. Kaduwela, C. S. Fadley, and M. A. Van Hove, Phys. Rev. B **50**, 6203 (1994).

[17] A. P. Kaduwela, H. Xiao, S. Thevuthasan, C. S. Fadley, and M. A. Van Hove, Phys. Rev. B **52**, 14 927 (1995).

[18] R. X. Ynzunza, H. Daimon, F. J. Palomares, E. D. Tober, Z. Wang, F. J. Garcia de Abajo, J. Morais, R. Denecke, J. B. Kortright, Z. Hussain, M. A. Van Hove, and C. S. Fadley, J. Electron Spectrosc. Relat. Phenom. **106**, 7 (2000).

[19] G. H. Fecher, Jpn. J. Appl. Phys. **38** (Suppl. 1), 582 (1999).

[20] Ch. Roth, H. B. Rose, F. U. Hillebrecht, and E. Kisker, Solid State Commun. **86**, 647 (1993); Ch. Roth, F. U. Hillebrecht, H. B. Rose, and E. Kisker, Phys. Rev. Lett. **70**, 3479 (1993).

[21] M. Getzlaff, Ch. Ostertag, G. H. Fecher, N. A. Cherepkov, and G. Schönhense, Phys. Rev. Lett. **73**, 3030 (1994).

[22] C. M. Schneider, U. Pracht, W. Kuch, A. Chasse, and J. Kirschner, Phys. Rev. B **54**, R15 618 (1996).

[23] A. Fanelsa, R. Schellenberg, F. U. Hillebrecht, E. Kisker, J. G. Menchero, A. P. Kaduwela, C. S. Fadley, and M. A. Van Hove, Phys. Rev. B **54**, 17 962 (1996); R. Schellenberg, E. Kisker, A. Fanelsa, F. U. Hillebrecht, J. G. Menchero, A. P. Kaduwela, C. S. Fadley, and M. A. Van Hove, *ibid.* **57**, 14 310 (1998).

[24] D. Venus, Phys. Rev. B **48**, 6144 (1993); **49**, 8821 (1994).

[25] G. H. Fecher, J. Braun, N. A. Cherepkov, L. V. Chernysheva, Th.

Jentzsch, J. Morais, A. Oelsner, Ch. Ostertag, J. Paul, H. Ufer, and G. Schönhense, Eur. Phys. J. B **11**, 161 (1999).
[26] N. A. Cherepkov, Phys. Rev. B **50**, 13 813 (1994).
[27] C. M. Schneider, D. Venus, and J. Kirschner, Phys. Rev. B **45**, 5041 (1992); D. Venus, L. Baumgarten, C. M. Schneider, C. Boeglin, and J. Kirschner, J. Phys.: Condens. Matter **5**, 1239 (1993); D. Venus, W. Kuch, A. Dittschar, M. Zharnikov, C. M. Schneider, and J. Kirschner, Phys. Rev. B **52**, 6174 (1995).
[28] F. U. Hillebrecht, H. B. Rose, T. Kinoshita, Y. U. Idzerda, G. van der Laan, R. Denecke, and L. Ley, Phys. Rev. Lett. **75**, 2883 (1995).
[29] C. M. Schneider, Z. Celinski, M. Neuber, C. Wilde, M. Grunze, K. Meinel, and J. Kirschner, J. Phys.: Condens. Matter **6**, 1177 (1994).
[30] C. S. Fadley, in *Synchrotron Radiation Research: Advances in Surface and Interface Science*, edited by R. Z. Bachrach (Plenum, New York, 1992).
[31] N. A. Cherepkov and G. H. Fecher, Phys. Rev. B **61**, 2561 (2000).
[32] S. Gorovikov, S. Bode, K. Starke, and G. Kaindl, J. Magn. Magn. Mater. **198-199**, 665 (1999).
[33] X. Gao, M. Salvietti, W. Kuch, C. M. Schneider, and J. Kirschner, Phys. Rev. B **58**, 15 426 (1998).
[34] K. Starke, E. Navas, L. Baumgarten, and G. Kaindl, Phys. Rev. B **48**, 1329 (1993).
[35] E. Arenholz, Ph.D. thesis, Wissenschaft & Technik Verlag, Berlin, 1996.
[36] D. Weller, S. F. Alvarado, W. Gudat, K. Schroeder, and M. Campagna, Phys. Rev. Lett. **54**, 1555 (1985).
[37] H. Tang, D. Weller, T. G. Walker, J. C. Scott, C. Chappert, H. Hopster, A. W. Pang, D. S. Dessau, and D. P. Pappas, Phys. Rev. Lett. **71**, 444 (1993), and references therein.
[38] Dongqui Li, L. Pearson, S. D. Bader, D. N. McIlroy, C. Waldfried, and P. A. Dowben, Phys. Rev. B **51**, R13 895 (1995).
[39] E. Weschke, C. Schuessler-Langeheine, R. Meier, A. V. Fedorov, K. Starke, F. Huebinger, and G. Kaindl, Phys. Rev. Lett. **77**, 3415 (1996).
[40] S. R. Mishra, T. R. Cummins, G. D. Waddill, K. W. Goodman, J. G. Tobin, W. J. Gammon, T. Sherwood, and D. P. Pappas, J. Vac. Sci. Technol. A **16**, 1348 (1998).
[41] E. D. Tober, F. J. Palomares, R. X. Ynzunza, R. Denecke, J. Morais, Z. Wang, G. Biino, J. Liesegang, Z. Hussain, and C. S. Fadley, Phys. Rev. Lett. **81**, 2360 (1998), and references therein; E. D. Tober, Ph.D. thesis, University of California Davis, 1997 (Lawrence Berkeley National Laboratory, Report No. LBNL-40442).
[42] A. Shick, W. E. Pickett, and C. S. Fadley, Phys. Rev. B **61**, R9213 (2000).
[43] G. Panaccione, P. Torelli, G. Rossi, G. van der Laan, M. Sacchi, and F. Sirotti, Phys. Rev. B **58**, R5916 (1998).
[44] Z. Hussain, W. R. A. Huff, S. A. Keller, E. J. Moler, P. A. Heimann, W. McKinney, H. A. Padmore, C. S. Fadley, and D. A. Shirley, J. Electron Spectrosc. Relat. Phenom. **80**, 401 (1996).
[45] C. S. Fadley, M. A. Van Hove, Z. Hussain, and A. P. Kaduwela, J. Electron Spectrosc. Relat. Phenom. **75**, 273 (1995).
[46] M. Farle, A. Berghaus, and K. Baberschke, Phys. Rev. B **39**, 4838 (1989).
[47] G. Andre, A. Aspelmeier, B. Schulz, M. Farle, and K. Baberschke, Surf. Sci. **326**, 275 (1995).
[48] A. Berger, A. W. Pang, and H. Hopster, J. Magn. Magn. Mater. **137**, L1 (1994).
[49] A. W. Pang, A. Berger, and H. Hopster, Phys. Rev. B **50**, 6457 (1994).
[50] E. D. Tober, R. X. Ynzunza, C. Westphal, and C. S. Fadley, Phys. Rev. B **53**, 5444 (1996).
[51] M. Farle and W. A. Lewis, J. Appl. Phys. **75**, 5604 (1994).
[52] R. Denecke, J. Morais, R. X. Ynzunza, J. G. Menchero, J. Liesegang, and C. S. Fadley, J. Electron Spectrosc. Relat. Phenom. **101-103**, 263 (1999).
[53] J. Henk, A. M. N. Niklasson, and B. Johansson, Phys. Rev. B **59**, 13 986 (1999).
[54] A. P. Kaduwela, D. J. Friedman, and C. S. Fadley, J. Electron Spectrosc. Relat. Phenom. **57**, 223 (1991).
[55] M. A. Van Hove, A. P. Kaduwela, H. Xiao, W. Schattke, and C. S. Fadley, J. Electron Spectrosc. Relat. Phenom. **80**, 137 (1996).
[56] J. G. Menchero, Phys. Rev. Lett. **76**, 3208 (1996).
[57] J. J. Rehr and R. C. Albers, Phys. Rev. B **41**, 8139 (1990).
[58] J. G. Menchero, Ph.D. thesis, University of California Berkeley, 1997 (Lawrence Berkeley National Laboratory, Report No. LBNL-40384).
[59] G. van der Laan, Phys. Rev. B **55**, 3656 (1997).
[60] M. P. Seah and W. A. Dench, Surf. Interface Anal. **1**, 2 (1979).
[61] V. Hinkel, L. Sorba, and K. Horn, Surf. Sci. **194**, 597 (1988).
[62] S. Tanuma, C. J. Powell, and D. R. Penn, Surf. Interface Anal. **11**, 577 (1988); **17**, 911 (1991).
[63] S. M. Goldberg, C. S. Fadley, and S. Kono, J. Electron Spectrosc. Relat. Phenom. **21**, 285 (1981).
[64] R. D. Cowan, *The Theory of Atomic Structure and Spectra* (University of California Press, Berkeley, 1981).
[65] R. D. Cowan, J. Opt. Soc. Am. **58**, 808 (1968); **58**, 924 (1968).
[66] G. H. Fecher, Europhys. Lett. **29**, 605 (1995).
[67] J. Braun, Rep. Prog. Phys. **59**, 1267 (1996).
[68] B. Ackermann and R. Feder, J. Phys. C **18**, 1093 (1985).
[69] J. B. Pendry, *Low Energy Electron Diffraction* (Academic, London, 1974); Surf. Sci. **57**, 679 (1976).
[70] R. Trehan, J. Osterwalder, and C. S. Fadley, J. Electron Spectrosc. Relat. Phenom. **42**, 187 (1987).
[71] Ch. Kittel, *Einführung in die Festkörperphysik* (R. Oldenbourg Verlag, München-Wien, 7. Aufl., 1988), and references therein.
[72] A. P. Kaduwela, D. J. Friedmann, and C. S. Fadley, J. Electron Spectrosc. Relat. Phenom. **57**, 223 (1991).
[73] J. Szade, M. Neumann, I. Karla, B. Schneider, F. Fangmeyer, and M. Matteucci, Solid State Commun. **113**, 709 (2000).
[74] J. Morais, G. H. Fecher, R. Denecke, J. Liesegang, and C. S. Fadley, J. Electron Spectrosc. Relat. Phenom. **114–116**, 783 (2001).
[75] D. A. Shirley, Phys. Rev. B **5**, 4709 (1972).
[76] W. J. Lademan, A. K. See, L. E. Klebanoff, and G. van der Laan, Phys. Rev. B **54**, 17 191 (1996).
[77] E. Arenholz, E. Navas, K. Starke, L. Baumgarten, and G. Kaindl, Phys. Rev. B **51**, 8211 (1995).
[78] S. P. Kowalcek, N. Edelstein, F. R. McFeely, L. Ley, and D. A. Shirley, Chem. Phys. Lett. **29**, 491 (1974).
[79] H. Osgasawara, A. Kotani, and B. T. Thole, Phys. Rev. B **50**, 12 332 (1994).
[80] H. Klar and H. Kleinpoppen, J. Phys. B **15**, 933 (1981).
[81] K. Blum, *Density Matrix Theory and Applications* (Plenum, New York, 1981).

[82] N. A. Cherepkov, Phys. Lett. A **40**, 119 (1972).
[83] Ch. Ostertag, J. Bansmann, Ch. Grünewald, Th. Jentzsch, A. Oelsner, G. H. Fecher, and G. Schönhense, Surf. Sci. **331-333**, 1197 (1995).
[84] M. Donath, B. Gubanka, and F. Passek, Phys. Rev. Lett. **77**, 5138 (1996).
[85] D. N. McIllroy, C. Waldfried, D. Li, J. Pearson, S. D. Bader, D.-J. Huang, P. D. Johnson, R. F. Sabiryanov, S. S. Jaswal, and P. A. Dowben, Phys. Rev. Lett. **76**, 2802 (1996).